IEEE Access
Multidisciplinary | Rapid Review | Open Access Journal

Received July 14, 2021, accepted August 1, 2021, date of publication August 31, 2021, date of current version September 10, 2021.

Digital Object Identifier 10.1109/ACCESS.2021.3109262

Magnetic Field Prediction of Module-Combined Stator Permanent Magnet Synchronous Motor Based on a Nonlinear Hybrid Analytical Model

YUNFEI LIU, BINGYI ZHANG, MING ZONG, GUIHONG FENG, AND BAOPING GAN
School of Electrical Engineering, Shenyang University of Technology, Shenyang 110870, China
Corresponding author: Bingyi Zhang (1392326904@qq.com)

ABSTRACT Module-combined stator permanent-magnet machines have several independent stator modules and each module can be controlled independently. To predict the magnetic field distribution of module-combined stator permanent-magnet machines accurately under asymmetric conditions, this paper proposes a novel nonlinear subdomain and magnetic equivalent circuit hybrid analytical model. The main novelty of the proposed nonlinear hybrid analytical model is representing nonlinear effect by equivalent current sheets on the edges of slots. Equivalent current densities are calculated from magnetic equivalent circuit and used as boundary conditions in the improved subdomain model. The values of the equivalent current sheets are obtained in an iterative algorithm. The nonlinear hybrid analytical model considering saturation effect can accurately calculate magnetic field distribution and electromagnetic performance even under overload conditions. The finite element analysis is performed to validate the accuracy of the proposed hybrid analytical model. A prototype with three stator modules is manufactured and the experimental results verified these predictions.

INDEX TERMS Magnetic field prediction, saturation effect, hybrid analytical model, module-combined stator, permanent magnet motor.

I. INTRODUCTION

Permanent magnet synchronous machines (PMSM) are widely used in many applications due to high efficiency and torque density. In some applications, higher reliability and fault tolerance of machines are required, such as railway traction drive, wind power generation, compressor application and electric aircraft [1]–[4]. Traditional permanent magnet machines do not have the ability of fault tolerance.

This article proposes a novel module-combined stator permanent magnet machine, which is consisted of several sector-shaped stator modules [5], [6]. The windings in each stator module have two kinds of span, which realize the independence of each module. Each stator module has its own independent inverter. Compared with conventional permanent magnet machines, module-combined stator permanent-magnet machines have better fault tolerance ability and are suitable for the applications that require higher reliability. When one stator module or its inverter fails to operate, the other modules can be in operation normally. In order to ensure the output torque unchanged, current in the wingdings of healthy modules should be increased. Then healthy modules operate under overload conditions, which will cause stator core seriously saturated. It is very important to predict magnetic field distribution accurately for analyzing the electromagnetic performances of module-combined stator permanent-magnet machines under asymmetric conditions.

There are four methods, FEA, analytical, magnetic equivalent circuit, hybrid method, to predict magnetic field distribution. FEA can predict magnetic field distribution accurately by considering saturation effect and the complex geometric models of machines [7], [8]. It is very time-consuming and the accuracy is depended on the quality of mesh. It cannot obtain results effectively with parameter variables, so it is not suitable for initial design of machines. Analytical method is an effective method to analyze the electromagnetic performances of machines. The conformal mapping method represents permanent magnet by equivalent current densities, and slotting effect is introduced by relative permeance function

The associate editor coordinating the review of this manuscript and approving it for publication was Kan Liu.

of air-gap [9], [10]. The subdomain model divides the whole machine into several solving regions. By applying interface and boundary conditions, the subdomain model solves the governing functions of each region and obtains all harmonic coefficient [11]–[13]. However, the disadvantage of the subdomain model is that it assumes that the core permeability is infinite and neglect the saturation effect. In [14], the relative permeability of core was taken into account in the analytical model, but permanent magnet is not considered. Magnetic equivalent circuit method can calculate the performance considering saturation effect. The whole motor is equivalent to a magnetic network which is composed of nonlinear reluctances with regular shape [15]–[17]. The accuracy of magnetic equivalent circuit method is poor compared with other analytical methods.

Some hybrid analytical models which combine conventional analytical methods and magnetic equivalent circuit method were presented. The hybrid models have the advantage of two methods. There are hybrid analytical models are based on the conformal mapping method [18]–[20]. However, these hybrid models cannot calculate slot leakage accurately. A hybrid model in [21] combines subdomain model and magnetic circuit model, however, the magnetic field in stator slots is predicted by the magnetic equivalent circuit method of the hybrid model, which cannot meet the precision. Subdomain and magnetic circuit hybrid model was proposed in [22] for open-circuit prediction, the magnetic field distribution is calculated based on the improved subdomain method of the proposed hybrid model. On-load magnetic field of permanent magnet machine was analyzed based on the hybrid model in [23]. However, the electromagnetic performances of permanent magnet machines under asymmetric conditions were not analyzed.

In this paper, the structure and power supply mode of the module-combined stator permanent-magnet machines is introduced. A nonlinear subdomain and magnet equivalent circuit hybrid analytical model is proposed for magnetic field distribution and electromagnetic performance prediction in module-combined stator permanent-magnet machines. The magnetic potential drop of nonlinear stator core can be represented by equivalent current densities on the edges of slots. Therefore, the nonlinear analytical model can be transformed to linear analytical model with equivalent current densities on the boundary of the slots. Equivalent current densities are obtained by magnetic equivalent circuit and used as boundary conditions in the improved subdomain model, and the flux sources flowing to the magnetic equivalent circuit are obtained by the improved subdomain model. The values of the equivalent current sheets are obtained in an iterative algorithm. According to the nonlinear magnetization curve of the core material, the relative permeability distribution of stator core at any time can be obtained. The nonlinear hybrid analytical model can accurately calculate air gap flux density, back EMF and electromagnetic torque. The electromagnetic characteristics of module-combined stator permanent magnet motor under asymmetric conditions are mainly analyzed. The finite element analysis is performed and a prototype is manufactured, the results of the proposed nonlinear hybrid analytical model show a good agreement with finite element results and experimental results.

II. MODULE-COMBINED STATOR

A. STATOR MODULE STRUCTURE

The stator of traditional permanent magnet machine is manufactured as a whole, which cannot be achieved modularization. The stator of module-combined stator permanent magnet machine is made into several sector modules and all modules are assembled. The stator structure of module-combined stator permanent magnet machine is shown in Fig. 1.

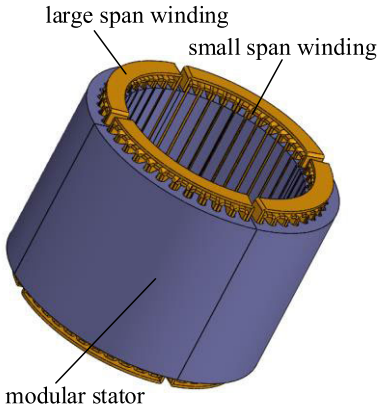

FIGURE 1. Structure of stator.

B. WINDING CONNECTION

The large and small span hybrid windings were introduced in each stator module. The independence of each stator module is achieved by the combination of the two unequal span windings. Compared with the traditional winding, the change is only the end wingding connection, the section in stator slot of winding is not changed. The diagram of wingding connection is shown in Fig. 2.

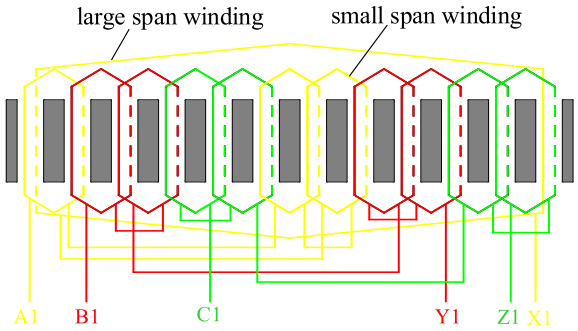

FIGURE 2. Winding connection of module stator.

The windings in each module are not connected to the wingdings in other modules. Each stator module is controlled independently by its own inverter. When one stator module or inverter fails, the other modules can continue to operate.

The novel module-combined stator permanent magnet machines have good ability of fault tolerance.

III. HYBRID ANALYTICAL MODEL

A. EQUIVALENCE OF ANALYTICAL MODELS

The principle that the saturation effect of stator core is considered in the analytical model is that the magnetic potential generated by the equivalent current on the boundary of the linear core is equal to the magnetic potential drop on the nonlinear stator core. Then, the nonlinear analytical model is equivalent to linear analytical by applying equivalent current densities on the slot edges. The saturation level of rotor yoke is usually not high. Therefore, equivalent current densities are only used on the boundaries of stator slot. The nonlinear analytical model and the equivalent linear analytical model are shown in Fig. 3.

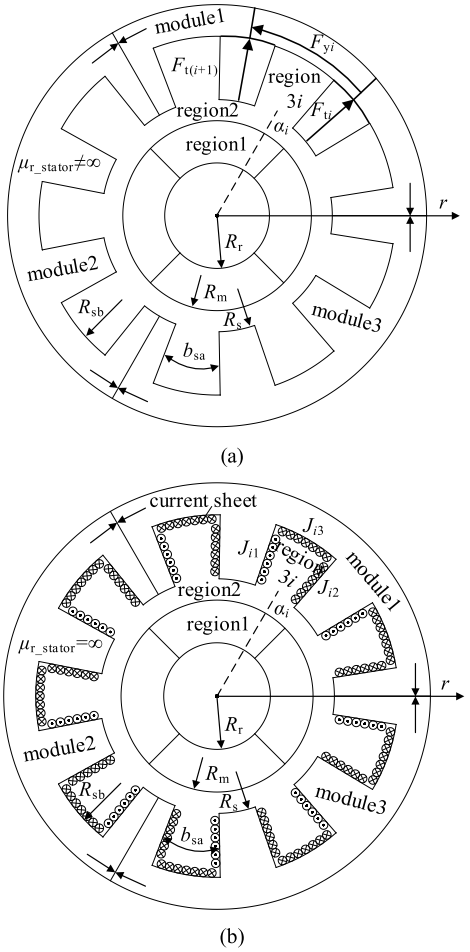

FIGURE 3. Equivalence of the two analytical models: (a) Nonlinear model; (b) Linear model with equivalent current sheets.

In Fig. 3, α_i is the center angle of the ith slot, b_{sa} is the angle of slot width, R_{sb}, R_s, R_m and R_r are the radius of slot bottom, slot opening, permanent magnet, rotor yoke, respectively, J_{i1}, J_{i2}, J_{i3} are the equivalent current densities on the ith stator slot edges, μ_0 and μ_r are the permeability of vacuum and stator core, respectively.

The nonoverlapping wingding layout is shown in Fig. 4. J_{ami1} and J_{ami2} are the current densities of the windings on both sides of the ith slot, d is the width of one winding side.

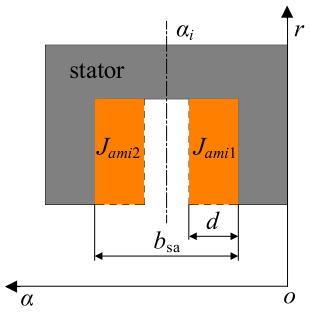

FIGURE 4. Winding layout.

B. IMPROVED SUBDOMAIN MODEL

The improved subdomain model is transformed to a linear model with equivalent current sheets on slot edges. Compared with traditional subdomain model, the boundaries conditions on slot edges in the improved subdomain model are not zero, they are replaced by equivalent current densities. The permeability of the core in the improved subdomain model is infinite, which is the same as the assumption of the traditional subdomain model. The basic assumptions of traditional subdomain model are applicable to improved subdomain model. The boundaries conditions on slot edges are modified to equivalent current densities, the analytical expressions have to be deduced.

1) MAGNETIC FIELD DISTRIBUTION IN SLOTS

The boundaries conditions on the ith slot edges are

$$H_{3ri}\left|_{\alpha=\alpha_i+b_{sa}/2}\right. = J_{i1} \tag{1}$$

$$H_{3ri}\left|_{\alpha=\alpha_i-b_{sa}/2}\right. = -J_{i2} \tag{2}$$

$$H_{3\alpha i}\left|_{r=R_{sb}}\right. = -J_{i3} \tag{3}$$

The vector potential in stator slot region satisfies Laplace equation. The general solution for nonoverlapping winding in slot is

$$A_{z3i}(r,\alpha) = A_{z3i0} + \sum_n A_{z3in}\cos\left[E_n\left(\alpha + b_{sa}/2 - \alpha_i\right)\right] \tag{4}$$

where

$$A_{z3in} = \left(B_{3n}G_3 - \frac{E_nW_nR_{sb}}{1-E_n^2} - \frac{2\mu_0J_{amn}R_{sb}^2}{E_n\left(E_n^2-4\right)}\right)\left(\frac{r}{R_{sb}}\right)^{E_n} + B_{3n}\left(\frac{r}{R_s}\right)^{-E_n} + \frac{rE_n^2W_n}{1-E_n^2} + \frac{\mu_0J_{amn}r^2}{E_n^2-4} \tag{5}$$

$$A_{z3i0} = \mu_0J_{am0}\left(2R_{sb}^2\mathrm{In}r - r^2\right)/4 + C_i\mathrm{In}r - \mu_0\left(J_{i1}+J_{i2}\right)r/b_{sa} + Q_{3i} \tag{6}$$

$$W_n = 2\mu_0\{-\left(J_{i1}+J_{i2}\right)(-1)^n$$

$$+J_{i2}[(-1)^n-1]\}/\left(E_n^2 b_{sa}\right) \tag{7}$$

$$C_i = R_{sb}\left[\mu_0 J_{i3}+\mu_0\left(J_{i1}+J_{i2}\right)/b_{sa}\right] \tag{8}$$

$$J_{iam0} = \left(J_{iam1}+J_{iam2}\right)/2 \tag{9}$$

$$J_{iamn} = 2\left(J_{iam1}-J_{iam2}\right)\sin\left(npi/2\right)/\left(npi\right) \tag{10}$$

$$E_n = npi/b_{sa} \tag{11}$$

$$G_3 = \left(R_s/R_{sb}\right)^{E_n} \tag{12}$$

where $Q_{3\,i}$ and $B_{3\,n}$ are the undetermined constants

Then, the radial and circumferential flux densities in slot region can be obtained by

$$B_{3ir}\left(r,\alpha\right) = \sum_n B_{3irn}\sin\left[E_n\left(\alpha+b_{sa}/2-\alpha_i\right)\right] \tag{13}$$

$$B_{3i\alpha}\left(r,\alpha\right) = B_{3i\alpha 0}+\sum_n B_{3i\alpha n}\cos\left[E_n\left(\alpha+b_{sa}/2-\alpha_i\right)\right] \tag{14}$$

where

$$B_{3irn} = -E_n\left\{\frac{E_n^2 W_n}{1-E_n^2}+\frac{\mu_0 J_{amn} r}{E_n^2-4}+\frac{B_{3n}}{R_s}\left(\frac{r}{R_s}\right)^{-E_n-1}+\left[\frac{B_{3n}G_3}{R_{sb}}+\frac{E_n W_n}{1-E_n^2}-\frac{2\mu_0 J_{amn}R_{sb}}{E_n\left(E_n^2-4\right)}\right]\times\left(\frac{r}{R_{sb}}\right)^{E_n-1}\right\} \tag{15}$$

$$B_{3i\alpha n} = -\left[\left(\frac{B_{3n}E_n G_3}{R_{sb}}-\frac{E_n^2 W_n}{1-E_n^2}-\frac{2\mu_0 J_{amn}R_{sb}}{\left(E_n^2-4\right)}\right)\times\left(\frac{r}{R_{sb}}\right)^{E_n-1}-\frac{B_{3n}E_n}{R_s}\left(\frac{r}{R_s}\right)^{-E_n-1}\frac{E_n^2 W_n}{1-E_n^2}+\frac{2\mu_0 J_{amn} r}{E_n^2-4}\right] \tag{16}$$

$$B_{3i\alpha 0} = -\frac{\mu_0 J_{am0}\left(R_{sb}^2/r-r\right)}{2}-\frac{C_i}{r}+\frac{\mu_0\left(J_{i1}+J_{i2}\right)}{b_{sa}} \tag{17}$$

2) MAGNETIC FIELD DISTRIBUTION IN MAGNET AND AIR-GAP

The solving process for magnetic field distributions in permanent magnetic and air-gap region are the same as traditional subdomain model. The detailed derivation process for the two regions is omitted in this article. The detailed derivation process and all coefficients can be found in [12].

The general solution in permanent magnetic and air-gap are

$$A_{z1} = \sum_k\left(C_{1k}A_1+C_{2k}M_{\alpha ck}-C_{3k}M_{rsk}\right)\cos\left(k\alpha\right)+\sum_k\left(C_{1k}C_1+C_{2k}M_{\alpha sk}-C_{3k}M_{rck}\right)\sin\left(k\alpha\right) \tag{18}$$

$$A_{z2} = \sum_k\left[A_2(r/R_s)^k+B_2(r/R_m)^{-k}\right]\cos\left(k\alpha\right)+\sum_k\left[C_2(r/R_s)^k+D_2(r/R_m)^{-k}\right]\sin\left(k\alpha\right) \tag{19}$$

The radial flux densities in permanent magnetic and air-gap are

$$B_{1r} = -\sum_k\left(k/r\right)\cdot\left(C_{1k}A_1+C_{2k}M_{\alpha ck}-C_{3k}M_{rsk}\right)\sin\left(k\alpha\right)+\sum_k\left(k/r\right)\cdot\left(C_{1k}C_1+C_{2k}M_{\alpha sk}-C_{3k}M_{rck}\right)\cos\left(k\alpha\right) \tag{20}$$

$$B_{2r} = -\sum_k\left(k/r\right)\cdot\left[A_2(r/R_s)^k+B_2(r/R_m)^{-k}\right]\sin\left(k\alpha\right)+\sum_k\left(k/r\right)\cdot\left[C_2(r/R_s)^k+D_2(r/R_m)^{-k}\right]\cos\left(k\alpha\right) \tag{21}$$

The circumferential flux densities in permanent magnetic and air-gap are

$$B_{1\alpha} = -\sum_k\left(1/r\right)\cdot\left(C_{4k}A_1+C_{5k}M_{\alpha ck}-C_{6k}M_{rsk}\right)\cos\left(k\alpha\right)-\sum_k\left(1/r\right)\cdot\left(C_{4k}C_1+C_{5k}M_{\alpha sk}-C_{6k}M_{rck}\right)\sin\left(k\alpha\right) \tag{22}$$

$$B_{2\alpha} = -\sum_k\left(k/r\right)\cdot\left[A_2(r/R_s)^k-B_2(r/R_m)^{-k}\right]\cos\left(k\alpha\right)+-\sum_k\left(k/r\right)\cdot\left[C_2(r/R_s)^k-D_2(r/R_m)^{-k}\right]\sin\left(k\alpha\right) \tag{23}$$

where A_1, C_1, A_2, B_2, C_2 and D_2 are undetermined coefficients. $C_{1\,k}$, $C_{2\,k}$, $C_{3\,k}$, $C_{4\,k}$, $C_{5\,k}$, $C_{6\,k}$, $M_{\alpha sk}$, $M_{\alpha ck}$, M_{rsk} and M_{rck} are known coefficients.

3) INTERFACE CONDITIONS

The interface and boundary conditions of all solving regions are

$$A_{z1}\left(R_m,\alpha\right) = A_{z2}\left(R_m,\alpha\right) \tag{24}$$

$$A_{z2}\left(R_s,\alpha\right) = A_{z3i}\left(R_s,\alpha\right) \tag{25}$$

$$H_{1\alpha}\left(R_m,\alpha\right) = H_{2\alpha}\left(R_m,\alpha\right) \tag{26}$$

$$H_{2\alpha}\left(R_s,\alpha\right) = H_{3\alpha i}\left(R_s,\alpha\right) \tag{27}$$

$$H_{1\alpha}\left(R_r,\alpha\right) = 0 \tag{28}$$

All undetermined coefficients can be obtained by applying these interface and boundary conditions.

C. MEC CONSIDERING SATURATION EFFECT

After the general solutions considering equivalent current sheets of all regions are obtained, it is necessary to accurately calculate current densities. The equivalent magnetic circuit of stator is shown in Fig. 5. The number of equivalent permeances in each stator tooth and yoke can be selected respectively according to the degree of nonlinearity effect.

The flux flowing into the nodes of equivalent magnetic circuit in Fig. 5 can be calculated from radial and circumferential flux densities in stator slot and air-gap by the improved

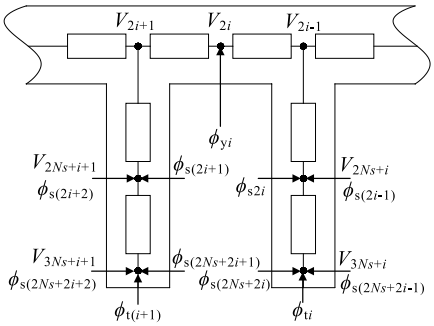

FIGURE 5. Magnetic equivalent circuit in stator slot.

subdomain analytical model

$$\phi_{sti} = R_s l_{ef} \int_{\alpha_i-\tau_t/2}^{\alpha_i-b_{sa}/2} B_{2r}(\alpha, R_s, t)d\alpha \tag{29}$$

$$\phi_{syi} = R_{sb} l_{ef} \int_{\alpha_i-b_{sa}/2}^{\alpha_i+b_{sa}/2} B_{3r}(\alpha, R_s, t)d\alpha \tag{30}$$

$$\phi_{ss2i} = l_{ef} \int_{(R_{sb}+R_s)/2}^{R_{sb}} B_{3\alpha}(\alpha_i + b_{sa}/2, r, t)dr \tag{31}$$

$$\phi_{ss(2i-1)} = -l_{ef} \int_{(R_{sb}+R_s)/2}^{R_{sb}} B_{3\alpha}(\alpha_i - b_{sa}/2, r, t)dr \tag{32}$$

$$\phi_{ss(2i+2N_s)} = l_{ef} \int_{R_s}^{(R_{sb}+R_s)/2} B_{3\alpha}(\alpha_i + b_{sa}/2, r, t)dr \tag{33}$$

$$\phi_{ss(2i+2N_s-1)} = -l_{ef} \int_{R_s}^{(R_{sb}+R_s)/2} B_{3\alpha}(\alpha_i - b_{sa}/2, r, t)dr \tag{34}$$

After all the flux sources flowing into the nodes are calculated, flux in branch of the equivalent magnetic circuit can be obtained by Kirchhoff's Current Law. The permeability of each tooth and yoke section is determined by flux passing through them. Then, the permeability of each section in stator is determined according to the B-H curve of iron core material. The B-H curve of iron core material is shown in Fig. 6.

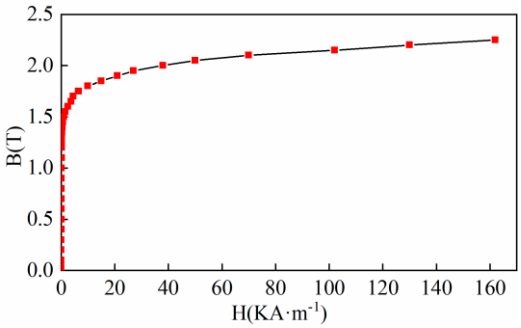

FIGURE 6. B-H characteristic of DW465-50.

Finally, the permeance of each tooth and yoke section can be calculated by the permeability and geometrical parameters. The magnetic potential matrix of nodes in equivalent magnetic circuit is

$$\mathbf{V} = \left(\mathbf{A}\boldsymbol{\Lambda}\mathbf{A}^{\mathbf{T}}\right)^{-1}\boldsymbol{\Phi} \tag{35}$$

where $\mathbf{A}$ is the incidence matrix, $\boldsymbol{\Lambda}$ is the permeance matrix, and Φ is the node flux matrix. The values of equivalent current densities on the ith stator slot edges can be calculated from nodes magnetic potential

$$J_{i1} = \left(V_{3N_s+i+1} - V_{2i+1}\right) / \left(R_{sb} - R_s\right) \tag{36}$$

$$J_{i2} = \left(V_{2i-1} - V_{3N_s+i}\right) / \left(R_{sb} - R_s\right) \tag{37}$$

$$J_{i3} = \left(V_{2i+1} - V_{2i-1}\right) / \left(R_{sb} \cdot b_{sa}\right) \tag{38}$$

where $R_{sb} - R_s$ and $R_{sb} \cdot b_{sa}$ are the lengths of each tooth and yoke, respectively.

D. COMBINATION OF MEC AND SUBDOMAIN

In the proposed hybrid analytical model, the equivalent current densities used as boundaries conditions in the improved subdomain model are calculated from equivalent magnetic circuit, and the flux sources flowing to the equivalent magnetic circuit are obtained by the improved subdomain model. Therefore, an iterative algorithm is required to find convergent solutions. The calculation flowchart of the proposed hybrid model is shown in Fig. 7. Then, magnetic field distributions and electromagnetic performances of module-combined stator permanent magnet machines can be calculated.

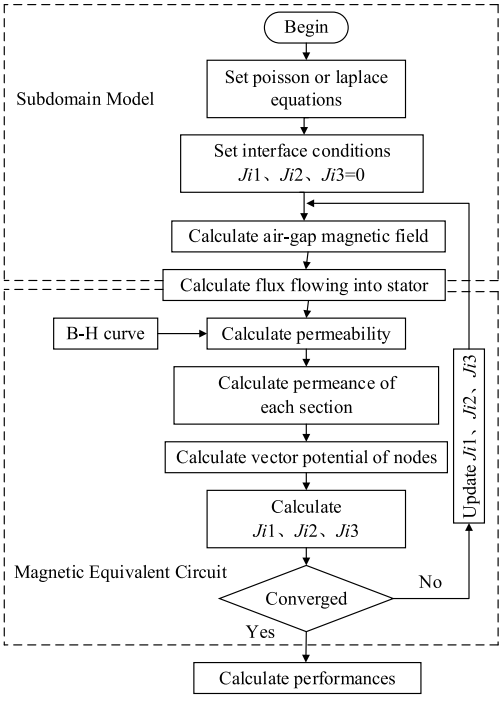

FIGURE 7. Calculation process of the hybrid model.

IV. FEA AND EXPERIMENT VALIDATION

In order to verify the effectiveness of the proposed hybrid analytical model, FEA is performed and a prototype with

three stator modules is manufactured. The main parameters of the prototype in shown in table 1.

TABLE 1. Main parameters of the prototype.

Parameter	Value
Number of slots	72
Number of poles	30
Number of modules	3
Slot bottom radius R_{sb} (mm)	229
Stator inner radius R_s (mm)	195
Magnet outer radius R_m (mm)	194.2
Rotor outer radius R_r (mm)	188.2
axial length L_{ef} (mm)	225
Number of turns	41
Pole-arc coefficient	0.88
Magnet remanence (T)	1.18
Slot width b_{sa} (degree)	2.77
Wingding width d (degree)	1.3

Fig. 8 shows the stator of prototype machine with three modules. Fig. 9 shows the flux density distributions of stator module with different current predicted by FEA, I, II and III are operated with 1, 1.5 and 3 times rated current, respectively.

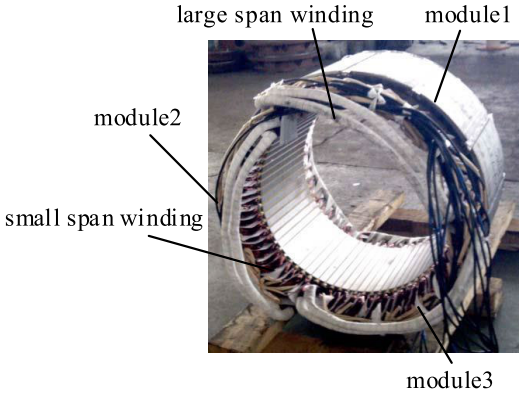

FIGURE 8. Stator of the prototype.

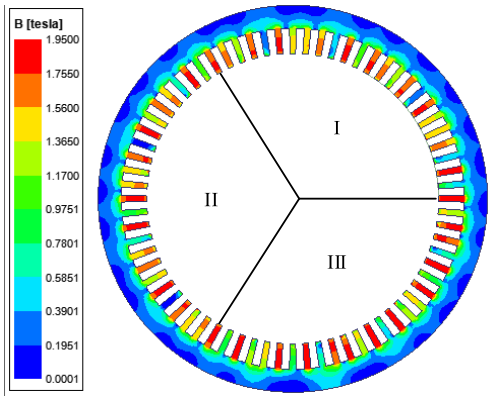

FIGURE 9. Flux density distribution of stator under load condition.

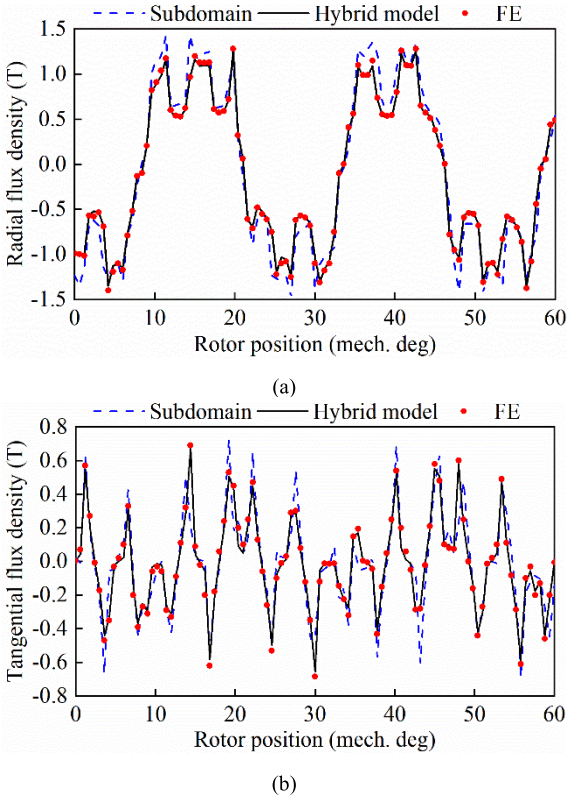

FIGURE 10. Air-gap flux densities: (a) Radial; (b) Tangential.

A. PERFORMANCES UNDER NORMAL CONDITIONS

Fig. 10 shows the radial and tangential flux densities in the middle of air-gap calculated by the conventional subdomain model, hybrid model and FEA method. The RMS value errors of radial and tangential flux densities of conventional subdomain model and finite element method are 4.3% and 4%, respectively. The RMS value errors of radial and tangential flux densities of the proposed hybrid analytical model and finite element analysis are 1.2% and 1.6%, respectively. The calculation results of the proposed hybrid analytical model have good consistency with FEA method. The conventional subdomain model cannot consider the nonlinearity effect, therefore, the results predicted by conventional subdomain overestimates.

Fig. 11 shows the back EMF predicted by three calculation methods mentioned above and the measured results. The results predicted by the hybrid analytical model are almost identical with FEA method. But the conventional subdomain model overestimates without taking saturation effect into consideration. The back EMF curves of measurement results and predictions by the proposed hybrid model and FEA match greet well, which verifies the high accuracy of the proposed hybrid analytical model with considering nonlinearity effect. The RMS values of the prediction by hybrid model and measured results are 218V and 215.7V, respectively. The error between the prediction of proposed hybrid analytical model

and the experiment results is 1.1% due to the manufacturing errors and without considering the end effect.

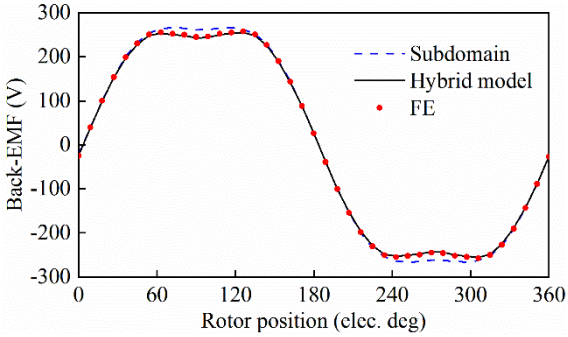

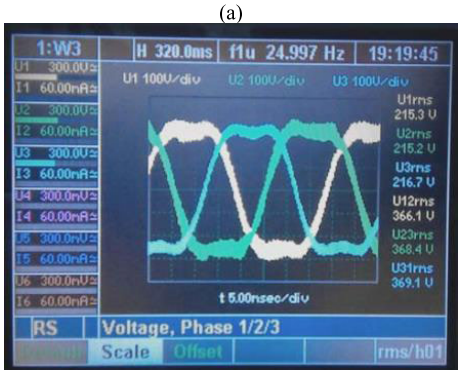

FIGURE 11. Phase no-load back EMF: (a) Calculated; (b) Measured.

Fig. 12 shows the electromagnetic torque predicted by the conventional subdomain model, hybrid model, FE model and the measurement. The hybrid model predictions are in good agreement with FEA results, while results predicted by the conventional subdomain are higher without taking saturation effect into account.

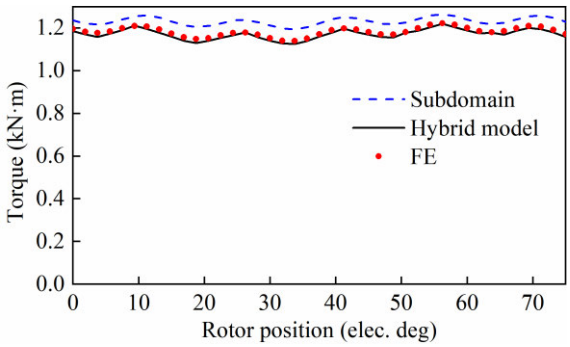

FIGURE 12. Electromagnetic torque.

B. TORQUE UNDER ASYMMETRIC CONDITIONS

When one stator module or the inverter fails during operation, the other modules can continue to operate without being affected. The module-combined stator permanent magnet machines have good ability of fault tolerance. In this section, the torque characteristics of the module-combined stator permanent magnet machine under asymmetric conditions are analyzed.

The electromagnetic torques with one and two modules in rated operation calculated by conventional subdomain model, the proposed hybrid model and FEA method are shown in Fig. 13. The average torque predicted by each method change linearly when different number stator modules are in rated operation. However, it cannot maintain the rated output torque.

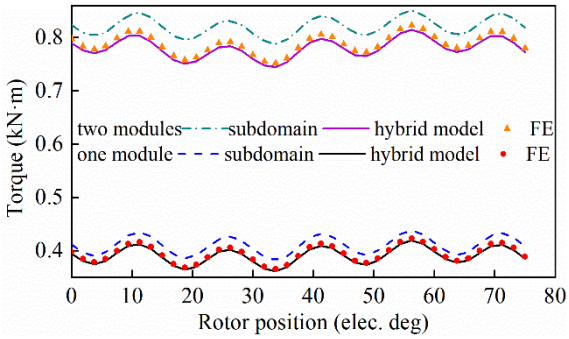

FIGURE 13. Torque with different modules in rated operations.

In order to maintain rated output torque unchanged, the current in the windings of modules in operation should be increased. When one and two modules are in operation, current need to be increased to 3 and 1.5 times, respectively. Fig. 14 shows torque with different modules in overload operations. Due to the neglection of saturation, the results calculated by conventional subdomain model are the same under different conditions. The results predicted by hybrid model and FEA model show a good agreement even under overload conditions. The difference between the conventional model and the proposed hybrid model is more significant when the saturation level is higher, which proves that the proposed hybrid model can accurately calculate the performances considering the nonlinearity effect. Due to the heavy saturation effect under overload conditions, the output torques of two modules with 1.5 times rated current in operation and one

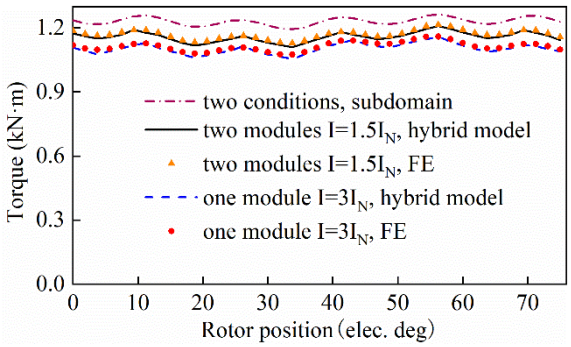

FIGURE 14. Torque with different modules in overload operations.

module with 3 times rated current in operation decrease to 98.9% and 94.2% of the rated torque, respectively.

Fig. 15 shows the experiment platform. The torques varied with current under different stator modules in operations are measured. As shown in Fig. 16, the predicted results by the proposed hybrid analytical model and the measured results have good agreement. The accuracy of the proposed hybrid analytical method even under heavy saturation conditions is verified.

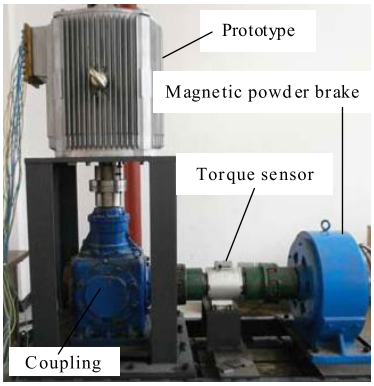

FIGURE 15. Experiment platform.

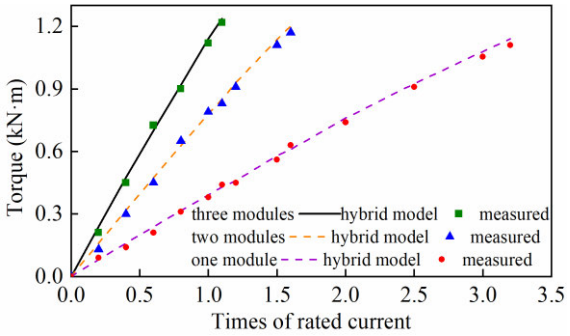

FIGURE 16. Torque varied with current.

V. CONCLUSION

This paper proposes a new nonlinear subdomain and magnetic equivalent circuit hybrid analytical model for magnetic field prediction in module-combined stator permanent-magnet machines. Saturation effect is considered by introducing equivalent current densities on the slot edges. The proposed hybrid model combines the advantages of the two analytical models. The nonlinear hybrid analytical model improved the accuracy compared to conventional linear model by considering saturation effect. It can reduce computational time significantly compared with finite element method. The results predicted by the proposed model, including air-gap flux densities, back-EMF and electromagnetic torque, match well with finite element results even under heavy saturation conditions. The experimental results of the prototype machine prove these predictions.

REFERENCES

[1] W. Wang, M. Cheng, B. Zhang, Y. Zhu, and S. Ding, "A fault-tolerant permanent-magnet traction module for subway applications," *IEEE Trans. Power Electron.*, vol. 29, no. 4, pp. 1646–1658, Apr. 2014.

[2] J. Li, K. T. Chau, J. Z. Jiang, C. Liu, and W. Li, "A new efficient permanent-magnet Vernier machine for wind power generation," *IEEE Trans. Magn.*, vol. 46, no. 6, pp. 1475–1478, Jun. 2010.

[3] Z. Kolondzovski, A. Arkkio, J. Larjola, and P. Sallinen, "Power limits of high-speed permanent-magnet electrical machines for compressor applications," *IEEE Trans. Energy Convers.*, vol. 26, no. 1, pp. 73–82, Mar. 2011.

[4] Y. Wang and W. Hao, "General topology derivation methods and control strategies of field winding-based flux adjustable PM machines for generator system in more electric aircraft," *IEEE Trans. Transport. Electrific.*, vol. 6, no. 4, pp. 1478–1496, Dec. 2020.

[5] B. Zhang, B. Gan, and Q. Li, "Analysis of a fault-tolerant module-combined stator permanent magnet synchronous machine," *IEEE Access*, vol. 8, pp. 70438–70452, Apr. 2020.

[6] B. Gan, B. Zhang, Q. Li, F. Guihong, and G. Li, "Research on operation of low-speed and high-torque module combined stator permanent magnetic fault-tolerant motor with unequal span winding," *IEEE Access*, vol. 8, pp. 166824–166838, Sep. 2020.

[7] S. Steentjes, S. Boehmer, and K. Hameyer, "Permanent magnet eddy-current losses in 2-D FEM simulations of electrical machines," *IEEE Trans. Magn.*, vol. 51, no. 3, pp. 1–4, Mar. 2015.

[8] M.-M. Koo, J.-Y. Choi, K. Hong, and K. Lee, "Comparative analysis of eddy-current loss in permanent magnet synchronous machine considering PM shape and skew effect using 3-D FEA," *IEEE Trans. Magn.*, vol. 51, no. 11, pp. 1–4, Nov. 2015.

[9] M. Hafner, D. Franck, and K. Hameyer, "Static electromagnetic field computation by conformal mapping in permanent magnet synchronous machines," *IEEE Trans. Magn.*, vol. 46, no. 8, pp. 3105–3108, Aug. 2010.

[10] D. Žarko, D. Ban, and T. A. Lipo, "Analytical solution for cogging torque in surface permanent-magnet motors using conformal mapping," *IEEE Trans. Magn.*, vol. 44, no. 1, pp. 52–65, Jan. 2008.

[11] F. Dubas and C. Espanet, "Analytical solution of the magnetic field in permanent-magnet motors taking into account slotting effect: No-load vector potential and flux density calculation," *IEEE Trans. Magn.*, vol. 45, no. 5, pp. 2097–2109, May 2009.

[12] L. J. Wu, Z. Q. Zhu, D. Staton, M. Popescu, and D. Hawkins, "An improved subdomain model for predicting magnetic field of surface-mounted permanent magnet machines accounting for tooth-tips," *IEEE Trans. Magn.*, vol. 47, no. 6, pp. 1693–1704, Jun. 2011.

[13] P. Jalali, S. T. Boroujeni, and N. Bianchi, "Simple and efficient model for slotless eccentric surface-mounted PM machines," *IET Electr. Power Appl.*, vol. 11, no. 4, pp. 631–639, Apr. 2017.

[14] Z. Djelloul-Khedda, K. Boughrara, F. Dubas, and R. Ibtiouen, "Nonlinear analytical prediction of magnetic field and electromagnetic performances in switched reluctance machines," *IEEE Trans. Magn.*, vol. 53, no. 7, pp. 1–11, Jul. 2017.

[15] D. Cao, W. Zhao, J. Ji, L. Ding, and J. Zheng, "A generalized equivalent magnetic network modeling method for vehicular dual-permanent-magnet Vernier machines," *IEEE Trans. Energy Convers.*, vol. 34, no. 4, pp. 1950–1962, Dec. 2019.

[16] L. Ding, G. Liu, Q. Chen, and G. Xu, "A novel mesh-based equivalent magnetic network for performance analysis and optimal design of permanent magnet machines," *IEEE Trans. Energy Convers.*, vol. 34, no. 3, pp. 1337–1346, Sep. 2019.

[17] M. M. Ghahfarokhi, A. D. Aliabad, S. T. Boroujeni, E. Amiri, and V. Z. Faradonbeh, "Analytical modelling and optimisation of line start LSPM synchronous motors," *IET Electr. Power Appl.*, vol. 14, no. 3, pp. 398–408, Mar. 2020.

[18] H. Saneie, Z. Nasiri-Gheidari, and F. Tootoonchian, "Design-oriented modelling of axial-flux variable-reluctance resolver based on magnetic equivalent circuits and Schwarz–Christoffel mapping," *IEEE Trans. Ind. Electron.*, vol. 65, no. 5, pp. 4322–4330, May 2018.

[19] A. Hanic, D. Zarko, and Z. Hanic, "A novel method for no-load magnetic field analysis of saturated surface permanent-magnet machines using conformal mapping and magnetic equivalent circuits," *IEEE Trans. Energy Convers.*, vol. 31, no. 2, pp. 740–749, Jun. 2016.

[20] Z. Li, X. Huang, L. Wu, T. Long, B. Shi, and H. Zhang, "Open-circuit field prediction of interior permanent-magnet motor using hybrid field model accounting for saturation," *IEEE Trans. Magn.*, vol. 55, no. 7, pp. 1–7, Jul. 2019.

[21] S. Ouagued, A. A. Diriye, Y. Amara, and G. Barakat, "A general framework based on a hybrid analytical model for the analysis and design of permanent magnet machines," *IEEE Trans. Magn.*, vol. 51, no. 11, pp. 1–4, Dec. 2015.
[22] L. Wu, H. Yin, D. Wang, and Y. Fang, "A nonlinear subdomain and magnetic circuit hybrid model for open-circuit field prediction in surface-mounted PM machines," *IEEE Trans. Energy Convers.*, vol. 34, no. 3, pp. 1485–1495, Sep. 2019.
[23] L. Wu, H. Yin, D. Wang, and Y. Fang, "On-load field prediction in SPM machines by a subdomain and magnetic circuit hybrid model," *IEEE Trans. Ind. Electron.*, vol. 67, no. 9, pp. 7190–7201, Sep. 2020.

YUNFEI LIU received the B.S. and M.S. degrees in electrical engineering and automation from Shenyang University of Technology, Shenyang, China, in 2014 and 2017, respectively, where he is currently pursuing the Ph.D. degree in electrical engineering. His research interests include the design and analysis of permanent magnet machines.

BINGYI ZHANG received the B.S., M.S., and Ph.D. degrees in electrical engineering from Shenyang University of Technology, Shenyang, China, in 1982, 1987, and 2007, respectively. He is currently a Professor with Shenyang University of Technology. His research interests include the design and optimization of electrical machines, low-speed high-torque drive systems, and power system automation.

MING ZONG received the B.S. degree in electrical engineering from Shenyang University of Technology, Shenyang, China, in 1982, the M.S. degree in electric drive and automation from Northeastern University, Shenyang, in 1995, and the Ph.D. degree in electrical engineering from Shenyang University of Technology, in 2007. He is currently a Professor with Shenyang University of Technology. His research interests include the design and control of special machines.

GUIHONG FENG received the B.S. degree in electrical engineering from Shenyang University of Technology, Shenyang, China, in 1985, and the M.S. degree in electric drive and automation from Northeastern University, Shenyang, in 1994. She is currently a Professor with Shenyang University of Technology. Her research interests include the design and optimization of electrical machines, low-speed high-torque drive systems, and power system automation.

BAOPING GAN received the B.S. degree in electrical engineering and automation from Shenyang University of Technology, Shenyang, China, in 2016, where he is currently pursuing the Ph.D. degree in electrical engineering. His research interests include the design and control of permanent magnet motors.